Food Packaging and Shelf Life xxx (xxxx) 101027

Contents lists available at ScienceDirect

Food Packaging and Shelf Life

journal homepage: www.elsevier.com/locate/fpsl

Biodegradable and active zein-gelatin-based electrospun mats and solvent-cast films incorporating sage extract: Formulation and comparative characterization

Ana Salević-Jelić [a], Steva Lević [a], Dušica Stojanović [b], Sanja Jeremić [c], Dunja Miletić [a], Milena Pantić [a], Vladimir Pavlović [a], Ivana Sredović Ignjatović [a], Petar Uskoković [b], Viktor Nedović [a]

[a] University of Belgrade, Faculty of Agriculture, Department of Food Technology and Biochemistry, Nemanjina 6, 11080 Belgrade, Serbia
[b] University of Belgrade, Faculty of Technology and Metallurgy, Department of Materials Science and Engineering, Karnegijeva 4, 11000 Belgrade, Serbia
[c] University of Belgrade, Institute of Molecular Genetics and Genetic Engineering, Laboratory for Molecular Genetics and Ecology of Microorganisms, Vojvode Stepe 444a, 11042 Belgrade, Serbia

ARTICLE INFO

Keywords:
Electrospinning
Solvent casting
Zein
Gelatin
Sage
Active biodegradable food packaging materials

ABSTRACT

This study aimed to develop active, biodegradable materials for food packaging by incorporating sage extract (SE) within a zein-gelatin blend by electrospinning and solvent casting. The fabrication techniques, SE incorporation, and its content (5, 10% w/w) determined the materials' properties. Electrospinning produced 0.36–0.53 mm thick, non-transparent fibrous mats (mean fiber diameter 1.12–1.36 μm). Solvent casting generated 0.34–0.41 mm thick, transparent continuous films. The analysis indicated the constituents' compatibility, homogenous dispersion, and efficient SE incorporation without strong chemical interactions and phase separation. The solvent-cast films presented more ordered structures, higher mechanical resistance, elongation, and water vapor barrier performance than the electrospun mats. The SE-incorporating formulations showed phenolics' delivery ability to food simulants influenced by structure, SE content, and media polarity. The electrospun mats expressed higher DPPH• radicals' inhibition, while the solvent-cast films showed stronger *Staphylococcus aureus* and *Escherichia coli* growth inhibition, increased by SE incorporation. All formulations showed rapid complete bio-disintegration in compost (18–25 days).

1. Introduction

The growing concerns about the abundant use of food plastic packaging are the use of non-renewable sources, low reusability and non-favorable balance between production and recycling, high waste quantity, improper disposal, long degradation periods, and environmental impact (Amin et al., 2022; Jayakumar et al., 2022). One of the extensive, innovation-driven research to tackle these issues and support sustainable development and circular economy focuses on biodegradable biopolymers for single-use and edible packaging materials. Interestingly, some biopolymers originate from the food industry by-products. Zein, a by-product of corn processing, is a promising biopolymer from environmental and economic viewpoints as low-cost, biodegradable, biocompatible, and generally recognized as safe (GRAS). It can generate coatings and films with low moisture absorption and high thermal resistance (Gagliardi et al., 2021; Gaona-Sánchez et al., 2015; Meng & Cloutier, 2014). The good film-forming properties of zein make its use as a coating material easy and practical, but as stand-alone material could face brittleness and lack of flexibility (Yemenicioğlu, 2016). An approach to address it is blending zein with other biopolymers, such as gelatin, a protein obtained by partial hydrolysis of collagen. Gelatin is abundant, biodegradable, biocompatible, and approved as GRAS with good film-forming properties and efficiency in improving the strength, flexibility, and handling of protein-based composite materials (Cao et al., 2007; Deng et al., 2018).

The development of biopolymer-based materials also focuses on food waste reduction. Accordingly, biopolymers can act as matrices incorporating active compounds to tailor an active role to the materials in

E-mail addresses: ana.salevic@agrif.bg.ac.rs (A. Salević-Jelić), slevic@agrif.bg.ac.rs (S. Lević), duca@tmf.bg.ac.rs (D. Stojanović), sanjajeremic@imgge.bg.ac.rs (S. Jeremić), dunjaduvnjak@gmail.com (D. Miletić), milenas@agrif.bg.ac.rs (M. Pantić), vlaver@agrif.bg.ac.rs (V. Pavlović), isredovic@agrif.bg.ac.rs (I.S. Ignjatović), puskokovic@tmf.bg.ac.rs (P. Uskoković), vnedovic@agrif.bg.ac.rs (V. Nedović).

https://doi.org/10.1016/j.fpsl.2023.101027
Received 16 September 2022; Received in revised form 25 December 2022; Accepted 4 January 2023
2214-2894/

food preservation, aiming to delay food quality and safety loss and increase shelf-life, preventing spoilage-caused waste. Thus, materials incorporating antioxidant and antimicrobial compounds aim to prevent oxidation reactions and microorganisms' growth (Amin et al., 2022; Jayakumar et al., 2022). Of importance to this end is zein compatibility with different active compounds (Mellinas et al., 2016). The focus is on natural actives, such as phenolic plant extracts, over synthetic preservatives due to safety requirements, the "clean labeling" trend, and bioactive properties (Amin et al., 2022; Núñez-Flores et al., 2013). The potent herb in this regard is sage (*Salvia officinalis* L.), widely used in dietary and medicinal preparations as a flavoring, preserving, and therapeutic agent. Sage extracts have many beneficial effects, including antioxidant, antifungal, and antibacterial, closely associated with phenolic constituents (Martins et al., 2014; Shan et al., 2007).

The fabrication of biopolymer-based materials incorporating natural active compounds endorses mild processing conditions to prevent denaturation. Solvent casting is a commonly used technique at a laboratory scale. It is simple and involves solubilization of film-forming constituents, casting the solution onto flat substrates, and drying under mild conditions, leading to film formation. As film manufacturing by solvent casting is batch, there are approaches to scale up the process and enable shorter and continuous production of bigger-size films (Etxabide et al., 2018; Mellinas et al., 2016). Another technique gaining increased interest is electrospinning. It implies electro-hydrodynamic processing, i.e., an action of a high-voltage electric field on polymer solution with active compounds, which makes charged jet of the solution from a spinneret tip and causes its elongation toward the grounded collector, resulting in mats composed of polymeric fibers incorporating actives. The advantages of electrospinning are continuous and facile process, ambient temperature and pressure conditions, cost-effectiveness, high specific surface of the fibers, and a possibility to scale up the process (Echegoyen et al., 2017; Etxabide et al., 2018). Either solvent casting or electrospinning could process solutions containing a blend of zein and gelatin, which defines the materials' properties (Deng et al., 2018). There are antibacterial electrospun gelatin/zein-based food packaging materials whose activity was provided by incorporating perillaldehyde (Wang et al., 2022) and resveratrol (Li et al., 2020). To the best of our knowledge, no studies dealing with active, biodegradable packaging materials based on zein-gelatin blend incorporating herbal extracts. Generally, materials based on biopolymers incorporating natural extracts are complex systems, and it is needed to define the phenomena of their structuring, possible interactions, and factors affecting their properties. Also, biodegradation of materials incorporating antimicrobial compounds is an important property but still not much explored.

This study aimed to develop biodegradable, active mats and films based on a zein-gelatin blend incorporating sage extract (SE). Initially, prepared SE was analyzed for phenolic compounds and then incorporated as an active constituent at different contents within the protein blend by electrospinning and solvent casting. Morphology, thickness, transparency, chemical interactions, thermal properties and stability, mechanical performance, water resistance, phenolics release, antioxidative and antibacterial potential, and degradation in a compost of the mats and films were studied to determine the effects of the applied fabrication technique, SE incorporation, and its content.

2. Material and methods

2.1. Materials

Plant material (*Salvia officinalis* L.) was from the Institute for Medicinal Plant Research "Dr. Josif Pančić" (Serbia). The matrix constituents were zein (Acros Organics, Belgium), gelatin (HiMedia Laboratories, India), and glycerol (NRK Engineering, Serbia). The solvents were acetic acid (Zorka Pharma-Hemija, Serbia), ethanol (Reahem, Serbia), formic acid (Merck KGaA, Germany), acetonitrile, and methanol (both Fisher Scientific, United Kingdom). The reagents were Folin-Ciocalteu (Merck KGaA, Germany), sodium carbonate (Fisher Scientific, United Kingdom), and 2,2-diphenyl-1-picrylhydrazyl (Sigma Aldrich, MA, USA). The standards were gallic acid (Merck KGaA, Germany), protocatechuic, ferulic, caffeic, *p*-coumaric acids (Sigma Aldrich, MA, USA), and rosmarinic acid (EDQM, France). The bacteria were from the American Type Culture Collection (ATCC, VA, USA), and the media (Müller Hinton Broth and Agar) were from HiMedia Laboratories (India).

2.2. Sage extract preparation

Maceration was performed with 50% (v/v) aqueous ethanol solution at a plant material-solvent ratio of 1:20 (w/v) on an orbital shaker (GFL 3005, Germany) at 200 rpm and room temperature for 90 min. The extraction solution was filtered and evaporated at 35 °C in a universal oven (UF55, Memmert GmbH + Co.KG, Germany) to obtain dry sage extract (SE). The extraction yield was determined using Eq. (1):

$$Yield\,(\%) = \frac{m_2}{m_1} \times 100 \quad (1)$$

where m_1 and m_2 are the weight (g) of the plant material subjected to the extraction and the produced dry extract, respectively.

2.3. Sage extract characterization

2.3.1. Total phenolics content (TPC) determination

TPC was determined using the Folin-Ciocalteu reagent (Singleton Vernon & Lamuela-Raventos, 1999). SE, reconstituted in 50% (v/v) aqueous ethanol solution (0.25 mL), was mixed in triplicate with Folin-Ciocalteu reagent (10-fold diluted in water, 1.25 mL). The mixture was placed in darkness at room temperature for five minutes, followed by Na_2CO_3 addition (75 g/L, 1 mL), and a reaction occurred for two hours in the dark at room temperature. The absorbance was measured at 760 nm using a UV-Vis spectrophotometer (HALO DB-20S, Dynamica Scientific Ltd., United Kingdom) against a blank containing the ethanol solution instead of the sample. TPC was determined using the gallic acid standard curve (0–100 mg/L) and expressed as mg gallic acid equivalents (GAE)/g SE.

2.3.2. High Performance Liquid Chromatography (HPLC) determination of phenolic acids (PAs)

PAs were identified and quantified by the Bischoff liquid chromatography system (Bischoff Chromatography, Germany) on a reversed-phase column (150×4.6 mm, 5 μm particle size, ProntoSIL 120–5-C18 AQ PLUS) and a UV-Vis detector. SE reconstituted in 50% (v/v) aqueous ethanol solution was filtered through a 0.45 μm nylon syringe filter and injected (20 μL) in triplicate. The mobile phase contained 0.2% (v/v) formic acid in water (A) and acetonitrile (B). The gradient elution for separation was applied according to Trifković et al. (2015) with slight modifications: 5–20% B (0–2 min), 20–55% B (2–20 min), 80% B (20–25 min), 80–100% B (25–30 min) at a flow rate of 0.8 mL/min. Protocatechuic, ferulic, caffeic, *p*-coumaric and rosmarinic acid were used standards. The detection wavelength was 290 nm, corresponding to a plateau wavelength range (290–305 nm) from the UV-Vis spectra of the standards (Supplementary material, Figure A.1). Identification of PAs of SE was made by comparing retention times and spectra with those of the standards and by spiking. The concentrations were determined using calibration curves of the standards (1–20 mg/L) and expressed as mg/g SE.

2.4. Synthesis of zein-gelatin-based mats and films

2.4.1. Preparation of solutions

Solutions based on a blend of zein and gelatin in 80% (v/v) aqueous acetic acid at a ratio of total biopolymer content to solvent of 3:7 (w/w) with zein to gelatin ratio of 3:1 (w/w) were prepared. There were four formulations:: control solution (without SE) and active solutions with different SE contents (5%, 10%, and 20% w/w, to the total biopolymer content). Each formulation contained glycerol (30% w/w to the total biopolymer content). Regarding the control solution preparation, zein was dissolved in an 80% (v/v) aqueous acetic acid solution under magnetic stirring at room temperature (2 h), followed by gelatin dissolution overnight. Finally, glycerol was added, stirring for one more hour. The active solutions preparation implied SE dissolution in the aqueous solution of acetic acid (80%, v/v) under magnetic stirring at room temperature overnight and filtration through 0.22 μm polytetrafluoroethylene (PTFE) filters, followed by dissolution of zein, gelatin, and glycerol in the filtrates as described for the control solution.

2.4.2. Electrospinning

The solutions-loaded syringes were placed on a pump and connected to a metallic stainless-steel needle with a 0.8 mm inner diameter through a PTFE tube. A positive electrode of a high-voltage power supply was attached to the needle. The electrospinning (CH-01 setup, Linari Engineering, Italy) occurred for one hour per cycle under a flow rate of 1.5 mL/h and a voltage of 23 kV in a sealed chamber at 20–25 °C and 50% humidity. The samples were collected on an aluminum foil placed over a grounded flat metallic collector and positioned 15 cm away from the needle tip. The designations used for the control electrospun formulation (without SE) and the active ones incorporating 5% and 10% SE were: ZGe, ZG-5SEe, and ZG-10SEe, respectively.

2.4.3. Solvent casting

The above-prepared solutions (7 g) were poured into plastic Petri dishes (9 cm diameter) and placed in a universal oven (UF55, Memmert GmbH + Co.KG, Germany) at 35 °C for 48 h. The designations used for the control solvent-cast formulation (without SE) and the active ones incorporating 5% and 10% SE were: ZGsc, ZG-5SEsc, and ZG-10SEsc, respectively.

2.5. Characterization of the electrospun mats and solvent-cast films

2.5.1. Morphology

After being coated with gold under vacuum on an SCD 005 sputter coater (BALT-TEC AG, Switzerland) morphology of the samples was analyzed by scanning electron microscopy (SEM) using a JSM-6390LV microscope (JEOL Ltd, Japan) at a voltage of 15 kV. The diameters of 100 fibers from 5 micrographs for each electrospun formulation were measured using the ImageJ program (National Institutes of Health, Bethesda, MD, USA).

2.5.2. Thickness

The thickness of three specimens for each formulation was measured at five points using an electronic caliper (pro-max Fowler, Fowler High Precision, MA, USA).

2.5.3. Transparency

The transparency of the samples was determined visually as contact transparency and quantitatively measuring the light absorption of three specimens (2× cm) set in the UV/Vis spectrophotometer cell (HALO DB-20S, Dynamica Scientific Ltd., United Kingdom) perpendicularly to the light beam. Transparency, *T*, was calculated following Eq. (2):

$$T(mm^{-1}) = A_{600}/L \quad (2)$$

where A_{600} is the absorbance measured at 600 nm, and *L* is the sample thickness (mm) (Malagurski et al., 2017).

2.5.4. Fourier transform infrared (FT-IR) spectroscopy

The chemical composition and effect of SE incorporation on structural properties of the mats and films, as well as chemical interactions between the constituents, were evaluated by FT-IR spectroscopy. The analysis was performed on the as-produced samples in attenuated total reflection mode (ATR), employing an IRAffinity-1S (Shimadzu, Japan). The spectra were recorded in the wavenumber range of 4000–600 cm^{-1} with a resolution of 4 cm^{-1} and 100 accumulations per scan and processed using software IR solution (Shimadzu, Japan) and Spectragryph (Menges, 2018).

2.5.5. Differential scanning calorimetry (DSC)

The thermal properties of the unloaded SE, mats, and films were evaluated by DSC using the DSC131 EVO instrument (Setaram Instrumentation, France). The samples sealed in aluminum pans were heated from − 40–250 °C at a heating rate of 10 °C/min under a nitrogen atmosphere.

2.5.6. Thermogravimetric analysis (TGA)

The thermal degradation behavior of the unloaded SE, mats, and films was tested by TGA, employing a TGA/DTA SETSYS 2400 CS Evolution instrument (Setaram Instrumentation, France). The temperature range was 25–700 °C at a heating rate of 5 °C/min under an argon flow rate of 20 mL/min.

2.5.7. Mechanical properties

The tensile test of the mats and films was performed using a Texture Analyzer Shimadzu EZ Test LX (Shimadzu, Japan). The specimens (40×10 mm) were stretched in triplicates with a jaws' distance of 20 mm at a crosshead speed of 30 mm/min at room temperature. The resulting stress-strain curves were used to determine tensile strength, elongation at break, and elastic modulus.

2.5.8. Water solubility, water contact angle, and water vapor permeability

The solubility of the mats and films in water was determined gravimetrically (Salević et al., 2022). The specimens (2× cm) in triplicates were dried in the universal oven (UF55, Memmert GmbH + Co.KG, Germany) at 105 °C to the constant weight (m_1) and then immersed in distilled water (25 mL). After 24 h of agitation at 100 rpm at room temperature on the orbital shaker (GFL 3005, Germany), the specimens were dried at 105 °C to the constant weight (m_2). The water solubility (*WS*) was calculated according to Eq. (3):

$$WS(\%) = \frac{m_1 - m_2}{m_1} \times 100 \quad (3)$$

The contact angle of water drops to the mats' and films' surfaces was determined using an optical microscope (Smart 5 MP Pro, Delta Optical, Poland) and the image analysis software (Algellai et al., 2018). To this end, distilled water (5 μL) was dropped at different positions on the surface of each sample in triplicates.

The mats' and films' water vapor permeability was determined gravimetrically (ASTM, 1995). The specimens in triplicates were sealed to the Payne permeability cups (5100, Elcometer, United Kingdom) filled with distilled water (5 mL) without direct contact between the specimens and water. The cups with the specimens without water and the cups with aluminum foil with water were tested as controls to evaluate the volatile compounds' loss and the water loss through the sealing, respectively. All cups were kept in a desiccator with dried silica gel on the bottom at 20 °C and weighed periodically for ten days. The water vapor permeability, *WVP*, was calculated following Eq. (4):

$$WVP(g/s \bullet m \bullet Pa) = \frac{WVTR \times L}{\Delta P} \quad (4)$$

where *WVTR* is the water vapor transmission rate determined from the permeation slope of weight loss as a function of time per unit of exposed specimen area (g/s•m^2), L is the sample thickness (m), and ΔP is the vapor partial pressure difference between the two sides of the specimens (Pa).

2.5.9. Migration test

The migration of phenolic compounds, as total phenolics and phenolic acids (particularly rosmarinic acid), from the mats and films into food simulant media: distilled water, 3% aqueous acetic acid solution (w/v), 10% and 95% aqueous ethanol solutions (v/v) was tested (European Commission, 2011; European Commission, 2017). The samples were immersed in triplicates into the media at a contact surface area-media ratio of 6 dm^2/kg and kept at 20 °C in darkness under static conditions. After ten days, the media were filtered through nylon filters (0.45 μm) and analyzed for total phenolic compounds and phenolic acids by the methodologies described in Sections 2.3.1. and 2.3.2, respectively. As proteins may contribute to the Folin-Ciocalteu test response, the absorbance of the media in contact with the control mats and films was measured and subtracted from the absorbance of the media with SE-incorporating ones.

2.5.10. Antioxidant activity

2,2-diphenyl-1-picrylhydrazyl (DPPH•) free radicals scavenging ability of the mats and films was determined to assess antioxidant potential (Salević et al., 2019). The samples were immersed in DPPH• methanolic solution (0.094 mmol/L) in triplicates at an equivalent 1 mg/mL and kept in darkness at room temperature under static conditions for 1 h. The control contained only the DPPH• solution. The absorbance was measured spectrophotometrically at 517 nm. DPPH• radicals' inhibition (I) was determined using Eq. (5):

$$I(\%) = \frac{A_c - A_s}{A_c} \times 100 \quad (5)$$

where A_c and A_s are the absorbance values of the control solution and the solution containing the sample, respectively.

2.5.11. Antibacterial activity

The broth macro-dilution assay (Malagurski et al., 2017) was applied to evaluate the antibacterial potential of the mats and films against *Staphylococcus aureus* ATCC 25923 and *Escherichia coli* ATCC 25922. Before adding the bacterial suspensions (preparation described in Supplementary material, Appendix 1), the samples were UV irradiation-sterilized (254 nm, 15 min each side). Tubes with the samples in the bacterial suspensions (concentration 320 mg/mL) were vortexed and incubated at 37 °C for 24 h under static conditions. Subsequently, serial dilutions of the suspensions were prepared and plated onto Müller Hinton Agar (37 °C for 24 h) to enumerate the remaining number of viable bacterial cells by counting colony-forming units (CFU). Tubes with the bacterial suspensions only were also prepared and treated as those containing the samples. The antibacterial activity was determined by calculating $\log_{10}(N_c/N_t)$, where N_c and N_t represent the average number of viable bacterial cells after the incubation without and with the samples, respectively.

2.5.12. Determination of released acetic-ion

The ion chromatography (IC) system Metrohm 761 Compact IC equipped with a chemical suppressor and thermostated conductivity detector (Metrohm, Switzerland) was employed to determine acetic-ion released from the mats and films into the suspensions during the incubation (details given in Supplementary material, Appendix 2).

2.5.13. Bio-disintegration in compost

Testing the bio-disintegration ability of the mats and films was performed in a compost model system according to the previously described protocol (Ponjavic et al., 2017). The samples (2×1.5 cm) were buried in duplicates (1 cm depth) inside glass Petri dishes (120 mm diameter, 30 mm height) containing the compost (100 g, 2 cm height) and placed for incubation (37 °C, 25 days). The humidity of the compost was maintained at around 50% by weight. The samples were periodically taken out, washed with hexane, dried, photographed, and weighed. The bio-disintegration was analyzed visually, comparing the appearance of the samples before and after the incubation. The bio-disintegration degree was also determined as weight loss by Eq. (6):

$$weightloss(\%) = \frac{m_i - m_r}{m_i} \times 100 \quad (6)$$

where m_i and m_r are the initial and residual sample weight (g), respectively.

2.6. Statistical analysis

The results, expressed as mean ± standard deviation, were statistically analyzed using SPSS Statistics 26 software (IBM, NY, USA). Depending on variance homogeneity tested by Levene's test, one-way analysis of variance (ANOVA) with posthoc Tukey's test or Kruskal-Wallis test with Mann-Whitney U test were employed to assess the influence of the extract incorporation and fabrication techniques on the properties of the mats and films. The significance level was $p < 0.05$.

3. Results and discussion

3.1. SE characterization: total phenolic content (TPC) and phenolic acids (PAs)

TPC and PAs were determined in the prepared sage extract (SE) to evaluate its potential to impart functionality to the electrospun mats and solvent-cast films, as these compounds are closely related to the antioxidant and antibacterial activity (Shan et al., 2007). The extraction yield of SE was 15.66% (w/w), with a TPC of 157.73 mg GAE/g SE. Among five identified (Supplementary material, Figure A.2) and quantified PAs, rosmarinic acid was the predominant (15.49 mg/g), followed by *p*-coumaric (2.33 mg/g), ferulic (1.18 mg/g), protocatechuic (0.87 mg/g), and caffeic (0.31 mg/g) acid. Several studies also reported *S. officinalis* extracts of different origins and applied extraction conditions as rich sources of phenolic compounds, with PAs being the major constituents. These studies also showed the dominance of rosmarinic acid among sage phenolic constituents, which is one of the quality parameters of sage extracts due to its many biological activities and potential health benefits (Farhat et al., 2013; Martins et al., 2014; Shan et al., 2005). The presence of these compounds in SE is of particular interest for active materials development due to their potent antioxidative and antimicrobial potential and low sensorial impact (Andrade et al., 2022; Hernández-García et al., 2022).

The SE was also analyzed by Fourier transform infrared (FT-IR) spectroscopy. The obtained spectrum (Fig. 1) showed the characteristic bands that we previously described (Salević et al., 2022). These are the broad band in the range of 3600–3000 cm^{-1} (phenolic O—H stretching vibrations, residual water), and the bands at around 2925 cm^{-1} (C-H stretching vibrations), 1715 and 1031 cm^{-1} (C=O and C—O stretching vibrations, respectively, attributed to extracted plant primary metabolites), and 1516 cm^{-1} (benzene ring stretching vibrations, assigned to secondary plant metabolites, primarily phenolic compounds).

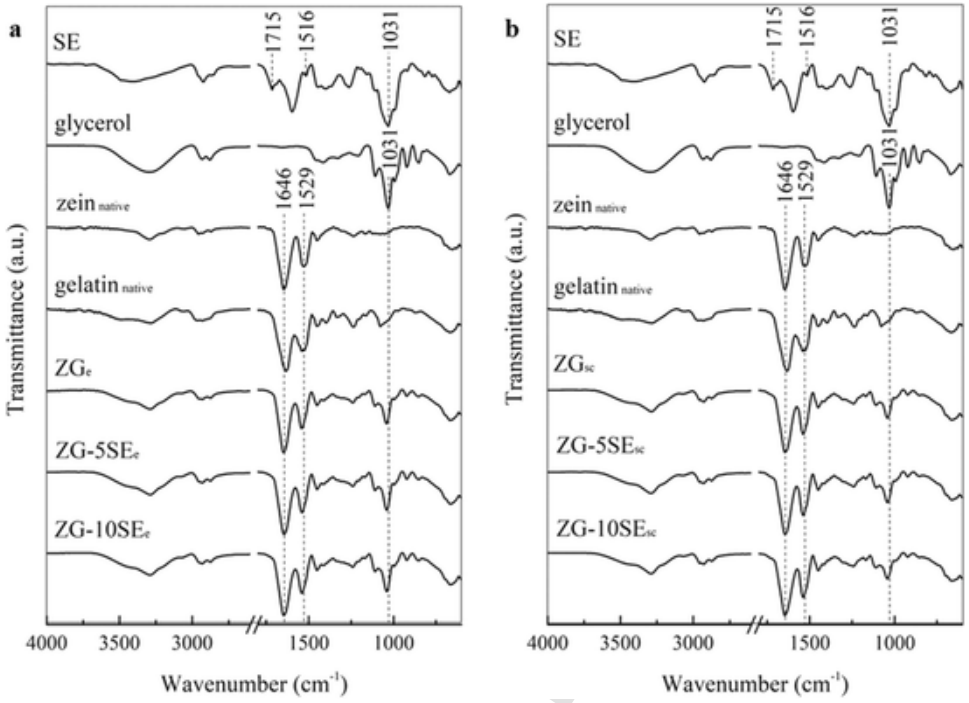

Fig. 1. FT-IR spectra of the constituents in native forms and the ZG-based electrospun mats (a) and solvent-cast films (b).

3.2. Characterization of the ZG-based electrospun mats and solvent-cast films

3.2.1. Morphology

The application of electrospinning and solvent casting techniques allowed the successful development of ZG-based mats and films, control ones (without SE), and those incorporating 5% and 10% (w/w) SE. The electrospinning process was stable and continuous, without the solutions dripping nor merging fibers. However, the increase in SE content to 20% (w/w) induced process instability and merging fibers, which excluded this formulation from the study.

The SEM micrographs (Fig. 2) depicted distinct differences in surface morphology and structure between the electrospun mats and solvent-cast films, regardless of the SE incorporation. The electrospinning technique produced mats composed of dense, randomly oriented, uniform fibers. Regardless of the SE incorporation and loaded content, the fibers presented similar morphologies with a regular, fibrillar shape and smooth surface without beads, aggregates, or defects. These morphological properties indicate a homogenous extract dispersion within the fibers (Salević et al., 2019). As shown in the diameter distribution histograms (Fig. 2), the SE incorporation and the higher loaded content increased ($p < 0.05$) the mean fiber diameter. Some studies also reported increased diameters of protein-based fibers after encapsulation of active compounds, such as zein fibers encapsulating gallic acid (5–20%) (Neo et al., 2013) and cross-linked gelatin/zein fibers encapsulating allopurinol (5–20%) (Deng et al., 2019). Considering that the processing parameters for the synthesis of all electrospun formulations in our study were the same, it may be assumed that the SE altered solution properties and interactions among the protein chains increasing fiber diameters. Active compounds may increase molecular entanglement in solution and impart jet resistance to the stretching forces during the electrospinning generating thicker fibers (Altan et al., 2018; Neo et al., 2013).

The solvent casting technique yielded structures of continuous and compact films. All solvent-cast formulations showed surface morphology with no pores, cracks, or phase separation, suggesting good constituents' compatibility and efficient SE incorporation within the film structures. There were wrinkled regions along the surfaces of all formulated films, which can be related to solvent evaporation. Of note, the solvent evaporation mode during solvent casting is surface-based, inducing molecular organization of polymers and forming solid film (Deng et al., 2018). Thus, solvent molecules during the drying diffuse slowly to the film-forming solution surface and evaporate there, which may cause the shrinkage of the film surface. Still, the wrinkled regions were less pronounced for the SE-incorporating films than for the control film. This observation implies that the SE may interact with the protein chains and affect their packaging, causing more homogenous deposits during the drying and smoother surfaces of the resulting films. Similarly, positive effects of natural extract incorporation on surface smoothness, homogeneity, and structure compactness of protein-based, solvent-cast films, were reported for gelatin films incorporating green tea extract (Wu et al., 2013).

3.2.2. Thickness

The electrospun formulations ZGe, ZG-5SEe, and ZG-10SEe were 364.67 ± 123.71, 488.67 ± 98.51, and 534.67 ± 123.55 μm thick, respectively. The SE incorporation increased the thickness ($p < 0.05$) compared to the control mat. This effect may be related to the mean diameter of the fibers making the mats. Thus, thicker fibers generated thicker mats, although the thickness of the mats loaded with 5% and 10% SE was similar ($p > 0.05$). The solvent-cast formulations ZGsc, ZG-5SEsc, and ZG-10SEsc were 341.33 ± 86.71, 397.33 ± 34.15, and 414.67 ± 89.80 μm thick, respectively. The SE incorporation and increase in its content slightly increased ($p > 0.05$) the thickness of the solvent-cast films indicating uniform SE distribution within the film structures.

3.2.3. Transparency

The developed ZG-based mats and films were visually homogeneous, without phase separation and defects, regardless of the fabrication technique and SE incorporation (Fig. 2). However, there were substantial differences in the visual appearance and contact transparency between the mats and films triggered by the fabrication techniques and discussed structural differences.

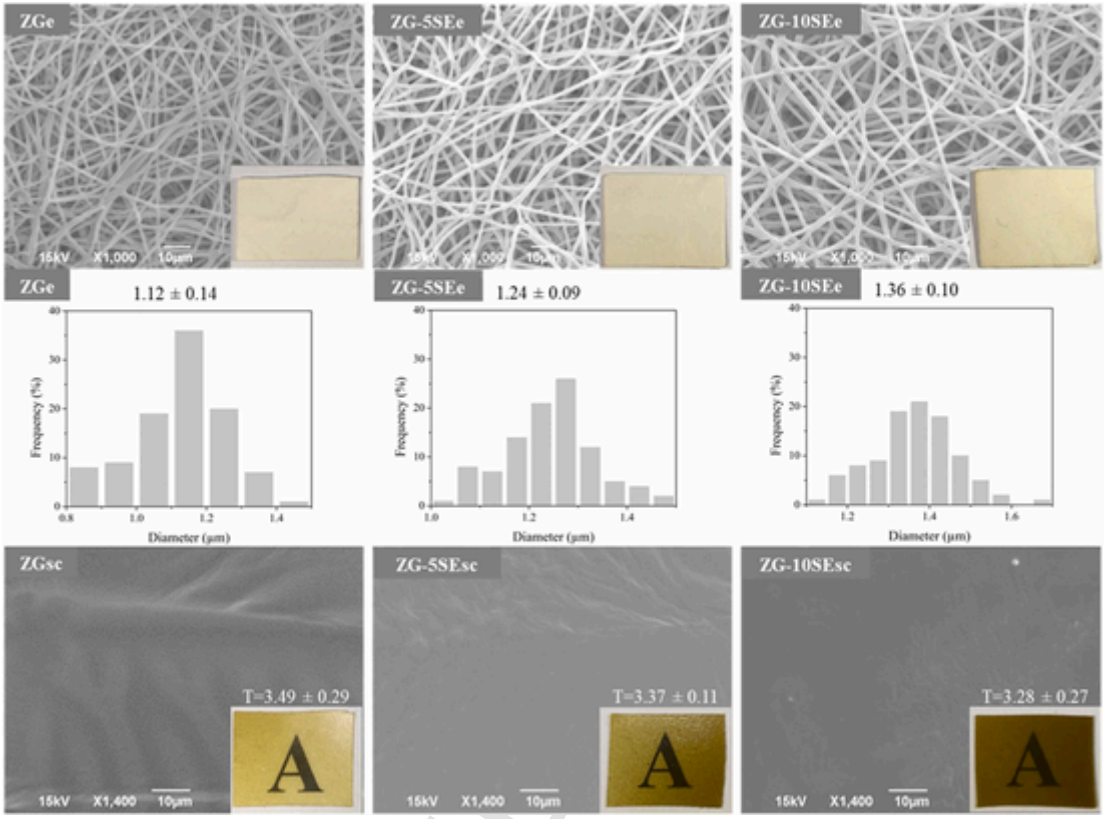

Fig. 2. SEM micrographs of the ZG-based electrospun mats (first row), histograms of fiber diameter distributions (second row), and SEM micrographs of the ZG-based solvent-cast films (third row). Macroscopic images of the mats and films showing their contact transparency and films' transparency values (T, mm^{-1}) are in the right bottom corner of the micrographs.

The electrospun mats were white-colored and opaque, regardless of the SE incorporation. As the mats are composed of thin, randomly oriented fibers generating porosity, the visual appearance is due to light scattering (Tijing et al., 2013). On the other hand, the compact and continuous structure of the solvent-cast films resulted in high contact transparency, regardless of the SE incorporation. The control film exhibited yellow color originating from the color of native zein. A darker color of the films was developed by the SE incorporation being more intense with the increase in the SE content due to the intrinsic SE color (Supplementary material, Figure A.3). Similarly, Gómez-Estaca et al. (2009) reported that oregano or rosemary extracts incorporation induced darker color of gelatin films. According to their findings, the darker coloration of the protein-based films incorporating herbal extracts is advantageous regarding light barrier properties, especially towards ultraviolet light, and thus against oxidation processes. However, the quantitative measurement of the transparency of the solvent-cast films developed in our study showed that the SE incorporation did not significantly alter the film transparency (Fig. 2) with similar transparency values for all solvent-cast formulations. These results may confirm compatibility among the film constituents and the ordered matrix. Generally, the visual appearance of the mats and films is an important property that determines their specific role. Regarding an application viewpoint as food packaging materials, the choice between the electrospun mats and solvent-cast films would depend on whether the packaging has to enable see-through or not.

3.2.4. FT-IR spectroscopy

Fig. 1 shows the spectra of the constituents in native forms and the developed mats and films. The spectra of the carriers exhibited typical bands for protein-based materials. The characteristic bands for zein are at 1646 (C═O stretching vibrations, amide I) and 1529 cm^{-1} (N—H bending and C—N stretching vibrations, amide II) (Neo et al., 2013). The spectrum of gelatin showed similar bands to those identified for zein but at different positions (i.e., amide I at 1634 cm^{-1}, amide II at 1539 cm^{-1}), demonstrating structural differences between these proteins. Glycerol had a strong band at 1031 cm^{-1} (C-O stretching) (Núñez-Flores et al., 2013).

The spectra of all electrospun mats and solvent-cast films were similar, presenting peaks like those identified for the constituents in native forms. The potential interactions are weak and reflected in overlapping the zein and gelatin bands, most probably occurring during the mats' and films' synthesis. The glycerol band at 1031 cm^{-1} shifted in the mats' and films' spectra (new position at ~1041 cm^{-1}), implying possible interactions between -OH groups of the plasticizer (glycerol) and the carriers (zein and gelatin) (Núñez-Flores et al., 2013; Wu et al., 2013). The SE incorporation did not induce new bands nor considerable shifts of the existing bands compared to the spectra of the control samples. The bands originating from the proteins and glycerol are only visible in the spectra of the SE-incorporating samples, completely overlapping the SE bands. In addition, there were no bands split in the spectrum of any mat and film. These spectral features indicate homogenous dispersion of the constituents and efficient, physical incorporation of SE within the ZG-based mats and films without strong chemical interactions to alter the FT-IR spectra.

3.2.5. DSC analysis

The effects of the fabrication techniques and SE incorporation on the thermal properties of the ZG-based electrospun mats and solvent-cast films were studied employing DSC. Fig. 3 gives DSC thermograms of the unloaded SE, mats, and films, and Table A.1 (Supplementary material) summarizes the corresponding data. The thermogram of the unloaded SE showed a broad endotherm peak at 100.13 °C and en-

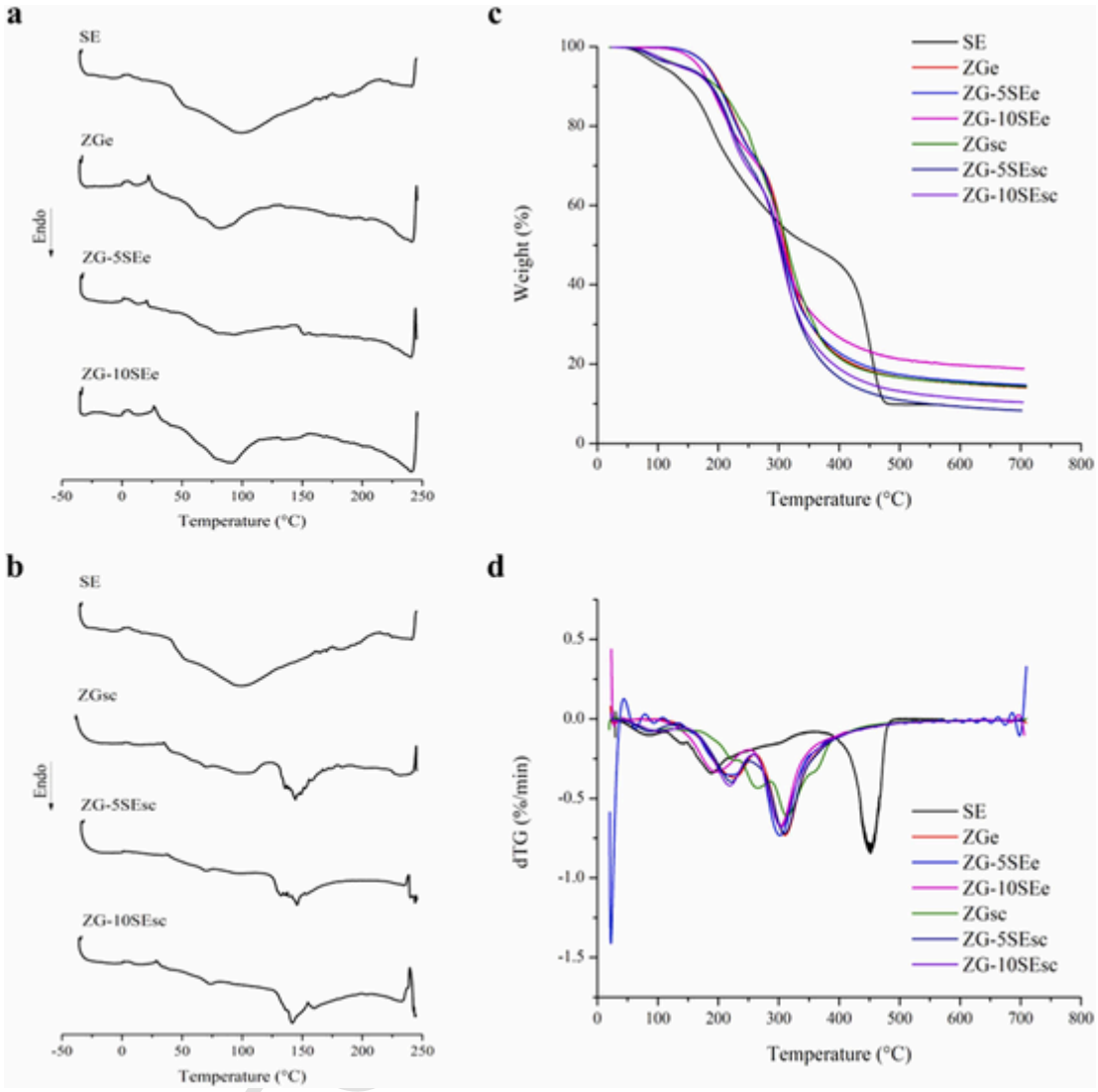

Fig. 3. DSC thermograms of the unloaded SE and the ZG-based electrospun mats (a) and solvent-cast films (b). TGA curves: weight loss as a function of temperature (c) and the first derivative analysis (d) of the unloaded SE and the ZG-based mats and films.

thalpy of 368.99 J/g, which can be related to the loss of solvent residues and volatile compounds.

Regarding the electrospun mats, the thermogram of the control showed an endothermic peak at 81.17 °C, representing denaturation temperature (Td) which is close to that reported by Deng et al. (2018) (83.77 °C) for the ZG-based electrospun mat at the same protein ratio. The SE incorporation within the mat at 5% loading induced only slight modifications of the thermal properties compared to the control mat, whereas 10% loading increased Td and ΔHd. This result suggests that the higher SE content incorporated within the mats triggered a more ordered structure that requires higher thermal energy for denaturation, which might be due to a potential hydrogen bonding of active compounds and protein matrix (Deng et al., 2019). Regarding the solvent-cast films, the thermogram of the control showed an endothermic peak at 144.29 °C, reflecting Td. The SE incorporation within the films slightly modified the thermal properties with similar Td and ΔHd for all film formulations, regardless of the SE incorporation, being in the range of 141.76–145.54 °C and 60.78–64.45 J/g, respectively (Supplementary material, Table A.1). The thermograms of ZGsc, ZG-5SEsc, and ZG-10SEsc also exhibited low-intensity endothermic peaks at 69.56, 69.67, and 73.50 °C, respectively, corresponding to their glass transition temperature. The increase in the glass transition temperature may reflect a more ordered system and the hydrogen bonding interactions between active compounds and proteins (Deng et al., 2019; Gaona-Sánchez et al., 2015). Altogether, the DSC analysis suggested that the higher content of the incorporated SE, rich in phenolic compounds, within the ZG-based mats and films promoted low-intensity interactions and more ordered structures, regardless of the fabrication technique.

A distinct difference in thermal properties of the samples, influenced by the fabrication technique, can be observed. The electrospun mats had lower Td than the respective solvent-cast films. This result could be due to the different solvent evaporation rates during the employed techniques, the electric field imposed on the solutions during the electrospinning, and the structural differences between the mats and films (Deng et al., 2019; Gaona-Sánchez et al., 2015; Krstić et al., 2017). Compared to the solvent casting technique, fast solvent evaporation and high stretching of the polymer chains during the electrospinning result in less ordered structures (Krstić et al., 2017). In this regard, the discussed SEM micrographs and the DSC analysis suggest that the compact, continuous structure of the solvent-cast films may stabilize their thermal properties compared to the fibrous structure of the electrospun mats. Also, the thermograms of the SE-incorporating samples, regardless of the fabrication technique and SE content, did not present

the SE-originating peak, which in agreement with the FT-IR analysis, indicates efficient SE incorporation. Finally, DSC analysis shows that the thermal properties of the ZG-based mats and films are primarily influenced by the fabrication technique, less by the SE incorporation.

3.2.6. TGA

TGA was used to study the effects of the fabrication techniques and SE incorporation on the thermal stability of the ZG-based electrospun mats and solvent-cast films. From TGA curves of the unloaded SE, mats, and films (Fig. 3), onset degradation temperature as the temperature at 5% weight loss, degradation temperature corresponding to the derivative peak maximum and subsequent weight loss, and residual mass at 700 °C were determined (Supplementary material, Table A.1).

The unloaded SE showed thermal stability behavior close to that we previously reported (Salević et al., 2019, Supplementary material, Appendix 3). In the thermal degradation curves of the mats and films, there were three weight loss stages. The onset degradation temperature at 5% weight loss (T5%) of the electrospun mats was in the range of 168–183 °C, which was higher than the one (136–143 °C) of the solvent-cast films. This weight loss could be due to the evaporation of adsorbed water, solvent residue, or SE volatiles. The temperature increase promoted the weight loss of the samples, and two peaks appeared. In dTG curves of the mats, these peaks appeared in the temperature range of 197–225 °C and 302–310 °C, with the weight loss range of 13–17% and 47–50%, respectively. Regarding dTG curves of the films, these peaks occurred in the temperature range of 219–265 °C and 304–314 °C, corresponding to the weight loss range of 20–28% and 50–55%, respectively. The first peak (Tdeg1) can be due to the loss of glycerol, structurally bound solvent, and decomposition of the mats and films. The second peak (Tdeg2), related to the maximum degradation rate, indicated the degradation of protein chains and SE (Contardi et al., 2017; Deng et al., 2018; Wu et al., 2013). Tdeg2 was similar for all formulations of the mats and films. Similarly, Liu et al. (2018) reported that ethyl cellulose-gelatine composites fabricated by either electrospinning or solvent casting had close temperatures of maximum weight loss. Also, Tdeg2 of the here-obtained ZG-based mats and films are similar to those reported for neat gelatin/zein nanofibers (Deng et al., 2018). Further temperature increase led to pyrolysis, providing residual mass at 700 °C in the range of 14–19% and 8–14% of the mats and films, respectively.

Compared to the control mat and film, the SE incorporation and increased loaded content decreased the decomposition temperature (Tdeg1), while the influence on the temperature of maximum degradation rate (Tdeg2) was lower. This behavior can be due to the evaporation of some SE volatile and low-molecular-weight compounds. Also, no SE-originating peaks were in the thermograms of the mats and films incorporating SE as being overlapped by those of the proteins. Therefore, TGA confirms the previous indications on efficient SE dispersion within the ZG-based mats and films without phase separation.

3.2.7. Mechanical properties

The tensile test was performed to determine the mechanical performance: tensile strength (TS), elongation at break (EAB), and elastic modulus (EM) of the developed mats and films as important properties for their practical use and ability to retain integrity during handling. As shown in Table 1, all ZG-based electrospun mats, control one and those incorporating SE, showed a low mechanical strength. The electrospun formulations withstood stress up to 0.87–0.95 MPa with elongation of 16–20% before the break and displayed elastic modulus in the range of 21–33 MPa. The SE incorporation within the fibers induced a slight ($p > 0.05$) increase in EAB and a decrease in EM compared to the control, implying a mild SE plasticizing effect on the resulting electrospun mats. Similarly, negligible interactions and a slight plasticizing effect were achieved with the SE incorporation within poly(ε-caprolactone) fibers (Salević et al., 2019).

Table 1
Mechanical properties (tensile strength (TS), elongation at break (EAB), and elastic modulus (EM)), water solubility (WS), and water vapor permeability (WVP) of the electrospun mats and solvent-cast films.

Sample	TS (MPa)	EAB (%)	EM (MPa)	WS (%)	WVP×10^{-10} (g/s•m•Pa)
ZGe	0.88 ± 0.11^{a}	16.17 ± 4.90^{ab}	32.85 ± 11.47^{a}	41.13 ± 0.44^{a}	48.9 ± 4.69^{a}
ZG-5SEe	0.95 ± 0.12^{a}	16.96 ± 3.28^{ab}	21.97 ± 5.63^{a}	36.78 ± 3.62^{bc}	42.9 ± 2.65^{a}
ZG-10SEe	0.87 ± 0.20^{a}	20.50 ± 2.17^{a}	21.47 ± 8.00^{a}	31.70 ± 1.40^{b}	36.3 ± 8.87^{a}
ZGsc	8.12 ± 1.19^{b}	14.67 ± 0.76^{b}	239.15 ± 95.10^{b}	43.82 ± 2.71^{d}	5.57 ± 0.48^{b}
ZG-5SEsc	1.14 ± 0.47^{a}	225.43 ± 166.74^{c}	26.32 ± 11.70^{a}	39.52 ± 0.71^{ac}	7.19 ± 0.49^{c}
ZG-10SEsc	3.07 ± 0.47^{c}	53.34 ± 12.82^{c}	82.06 ± 19.60^{c}	34.44 ± 0.69^{b}	5.44 ± 0.54^{b}

Different letters within the same column indicate significant differences among formulations ($p < 0.05$).

The solvent-cast films showed higher TS (1–8 MPa), EAB (15–225%), and EM (26–239 MPa), i.e., higher resistance to stress, elongation that can withstand before the break, and stiffness than the electrospun mats. Concerning the discussed structural differences, i.e., the porosity of the electrospun mats and the compactness of the solvent-cast films, this result could be expected. It pointed out that the mats' and films' mechanical performance is related to their structure and induced by the fabrication techniques. The same effect of electrospinning and solvent casting techniques on the mechanical behavior of the resulting mats and films was shown for synthetic polymer (Tijing et al., 2013).

The applied fabrication techniques also provided different extents of the SE effects on the mechanical behavior of the here-developed mats and films. A more pronounced SE plasticizing effect was determined for the solvent-cast films, improving their deformability and flexibility. Compared to the control solvent-cast film, the SE incorporation significantly ($p < 0.05$) decreased TS and EM and increased EAB, resulting in films being less breaking-resistant, less stiff, and more extensible. Accordingly, it may be assumed that slow solvent evaporation during the solvent casting allowed the SE to interact with the protein chains and affect their packaging, giving rise to higher chains' mobility and favoring films' elasticity. Similarly, Rasid et al. (2018) reported increased EAB of protein-based films when incorporating phenolics-rich extract. They ascribed this effect to altered film structure, potential phenolics-protein interactions, and extract-protein compatibility, resulting in more cohesive and flexible film matrices. Liu et al. (2019) also reported a plasticizing effect of phenolics on protein-based films. However, it can be observed that the ZG-10SEsc had a higher strength and stiffness than the ZG-5SEsc. This effect may be due to more probable interactions between the proteins and SE present in the higher content, leading to film strengthening and compactness. In this regard, phenolics-proteins interchain interactions may reduce the plasticizing effect and thus decrease flexibility (Zhang et al., 2019). This implication is in line with the SEM micrographs (Fig. 2), where the most compact and homogenous film surface was observed for the ZG-10SEsc formulation.

Regarding the potential of using the mats and films as packaging materials, the obtained results suggest that the solvent-cast films would be more appropriate as stand-alone materials, being more able to withstand stress during handling. On the other hand, the electrospun mats could be applied directly on food surfaces as coatings or could be subjected to post-processing treatments, such as pressing and annealing, to improve their mechanical properties.

3.2.8. Water solubility, water contact angle, and water vapor permeability

The behaving property of the mats and films in a high-water content environment was evaluated regarding water solubility, water contact angle, and water vapor permeability as a function of the SE incorporation and fabrication techniques.

The water solubility (WS) of materials is an important property that reflects their water resistance. Within the solubility test, all mats' and films' formulations showed great integrity, not being readily soluble. As seen in Table 1, the solvent-cast films showed somewhat higher WS than the corresponding electrospun mats, which can be due to the discussed higher flexibility, i.e., higher chains' mobility of the solvent-cast films, facilitating their solubility. However, the SE incorporation had a more pronounced effect on the mats' and films' WS than the fabrication techniques. There was a decreasing trend in the mats' and films' WS with the SE incorporation and the increase in its content. This is consistent with other studies reporting decreased WS of films based on gelatin-containing biopolymers-blend when incorporating phenolics-rich extracts (Bertolo et al., 2022; Tagrida et al., 2023). It can be attributed to the competing effect of the extract phenolic compounds with water molecules, where phenolics may interact with protein chains, decreasing their hydrophilic sites, availability, and affinity for water binding. Also, it was shown that rosmarinic acid decreased the WS of gelatin films, relating the hydrophobicity to the benzene ring (Zhang et al., 2019).

The water contact angle (WCA) on the surface of materials reflects their wettability and hydrophilicity/hydrophobicity. The images of a water drop applied on the mats' and films' surfaces are gathered in the Supplementary material (Fig. A.4.). All mats' and films' formulations showed low WCAs, indicating their hydrophilic character. Comparing the control formulations, the electrospun mat showed higher hydrophobicity (WCA 34.47°) than the solvent-cast film (WCA 22.81°). According to Deng et al. (2018), the differences in WCAs of the mats and films could be due to different solvent evaporation mechanisms during manufacturing, influencing orientations of proteins' hydrophobic/hydrophilic domains. During fast solvent evaporation of electrospinning, there is a concentration gradient of proteins from the surface to the core within unsolidified fibers with the maximum concentration at the air-liquid interface. Hence, proteins solidify from outside to inside, where the nonpolar air side causes the orientation of proteins' hydrophobic domains outside. On the other hand, surface-mediated evaporation of solvent casting forms a concentration gradient where solvent molecules move to the solution surface, i.e., the air-liquid interface, and evaporate there. In this case, the proteins' solidification occurs from inside to outside, orientating the proteins' hydrophilic domains outside. The higher WCAs were also reported for ethyl cellulose, ethyl cellulose-gelatin blend (Liu et al., 2018), and polyurethane (Tijing et al., 2013) electrospun mats compared to the respective solvent-cast films. Interestingly, the SE-incorporating mats showed immediate water absorption, not enabling WCA measuring. As discussed, the SE incorporation increased fibers' diameters, which may decrease tortuous paths and facilitate water absorption. Similarly, Deng et al. (2018) reported an immediate disappearance of a water drop on gelatin nanofibers' surface. Concerning the solvent-cast films, the SE incorporation increased WCAs to 29.69 and 25.99° for the films incorporating 5% and 10% SE, respectively. The greater hydrophobicity of the SE-incorporating films than the control one is in line with their lower WS.

Concerning the application of interest as food packaging materials, aiming to preserve food quality and extend shelf-life, water vapor permeability (WVP) of materials is an important property reflecting their barrier performance against moisture transfer between food and surrounding. As one can observe (Table 1), electrospinning and solvent casting generated the mats and films with the significantly different ($p < 0.05$) WVP, where the solvent-cast films showed lower WVP values. This result could be ascribed to the structural differences, where the fibrous structure of the electrospun mats generates porosity and thus makes paths for water sorption and easier permeation than the continuous, compact structure of the solvent-cast films. The SE incorporation and increase in its content slightly improved ($p > 0.05$) water vapor barrier performance of the mats. The slight SE influence on the mats' WVP is in line with the similar morphological properties of all electrospun formulations and homogenous SE dispersion within the fibers. Regarding the solvent-cast films, the SE incorporation at 5% content significantly increased ($p < 0.05$) the WVP, while 10% content provided the same WVP order of magnitude as the control solvent-cast film. This result could be related to the SE plasticizing effect on the solvent-cast films observed in the mechanical properties analysis. Accordingly, the strong SE plasticizing effect at 5% content may increase the chains' mobility and free volume through the matrix, making it more available for water permeation. Detrimental influence on water vapor barrier performance was also reported for other materials incorporating active constituents with plasticizing effect at lower loadings (Melendez-Rodriguez et al., 2019). However, the water vapor barrier performance improvement at 10% content of the incorporated SE may be due to the discussed reduction in the plasticizing effect at the higher SE content and the above-shown most compact and homogenous morphology of ZG-10SEsc. Interestingly, the here-developed ZG-based mats and films presented a lower WVP than the widely used commercial polyvinyl chloride (PVC) wrap film (2.61×10^{-6} g•mm/h•cm•Pa) (Kaewprachu et al., 2015), implying their potential for packaging applications.

3.2.9. Migration

An important property of materials for active food packaging applications is the ability to release active compounds into foods when in direct contact. Accordingly, the migration potential of phenolics from the mats and films into 3% (w/v) aqueous acetic acid solution (AA), distilled water (W), 10% and 95% (v/v) aqueous ethanol solutions (10%E and 95%E, respectively) was studied. These media represent food simulants for food with a hydrophilic character and food with pH below 4.5 (AA), a hydrophilic character (W, 10%E), and a lipophilic character (95%E). The test was performed by total immersion of the samples into the media for ten days at 20 °C, corresponding to the contact conditions of 3–30 days at 5–20 °C in the worst foreseeable use (European Commission, 2011; European Commission, 2017). The samples retained integrity over the test with the incorporated SE content, samples' structure, and media polarity influencing phenolics migration from the ZG-based mats and films to the food simulants (Table 2). Among PAs determined in the unloaded SE (Section 3.1), rosmarinic acid (RA) was the only detected in the media. As expected, there was higher migration

Table 2
Migration of phenolics from the ZG-based mats and films to the food simulant media: 3% (w/v) acetic acid (AA), distilled water (W), 10% (v/v) ethanol (10%E), and 95% (v/v) ethanol (95%E).

Sample	AA	W	10%E	95%E
	Total phenolic compounds (mg GAE/kg media)			
ZG-5SEe	13.42 ± 3.83^{a1}	10.03 ± 0.81^{ab1}	15.42 ± 0.70^{a1}	22.18 ± 0.56^{a2}
ZG-10SEe	26.67 ± 5.82^{ab1}	28.78 ± 1.78^{c1}	27.46 ± 0.59^{b1}	32.13 ± 2.31^{b1}
ZG-5SEsc	20.80 ± 2.99^{ac1}	15.04 ± 9.42^{ac1}	12.02 ± 0.50^{ac1}	11.93 ± 0.52^{c1}
ZG-10SEsc	29.99 ± 5.00^{bc12}	46.80 ± 10.89^{d1}	20.33 ± 0.72^{ad2}	20.94 ± 0.76^{a2}
	Rosmarinic acid (mg RA/kg media)			
ZG-5SEe	n.d.	n.d.	n.d.	2.12 ± 0.55^{a}
ZG-10SEe	n.d.	1.77 ± 0.05^{a1}	1.78 ± 0.48^{a1}	9.22 ± 2.43^{b2}
ZG-5SEsc	n.d.	n.d.	n.d.	n.d.
ZG-10SEsc	n.d.	3.43 ± 0.05^{b1}	1.08 ± 0.18^{b2}	6.43 ± 0.00^{c3}

Different letters within the same column indicate significant differences among formulations ($p < 0.05$).
Different numbers within the same row indicate significant differences among media ($p < 0.05$).
n.d. not detected

of phenolic compounds, determined as total, and RA from the samples incorporating the higher SE content, regardless of the technique and medium.

There was a different trend of migration of phenolic compounds determined as total from the mats and films into the food simulants. In the case of the electrospun mats, there were slight variations in the phenolics' migration into AA, W, and 10% E, while the highest amounts migrated to 95%E. The high content of non-polar amino acid residues, water-insolubility, and solubility in aqueous ethanol of zein, as well as gelatin insolubility in water at 20 °C (Meng & Cloutier, 2014), may induce higher susceptibility of the mats, and consequently the higher migration of the actives to less polar solvents, in this case to 95% ethanol. On the other hand, the solvent-cast films showed the lowest phenolics migration into the ethanol-containing media. The phenolics' migration from the films increased in AA, which may be due to proteins' protonation by the acid (Li et al., 2020). The highest migration occurred in distilled water. This migration behavior is in line with the previous observation (Section 3.2.8) that the different solvent evaporation mechanisms during electrospinning and solvent casting induce different orientations of the proteins' hydrophobic/hydrophilic domains (Deng et al., 2018). Thus, the orientation of proteins' hydrophobic domains outside during electrospinning and hydrophilic domains outside during solvent casting induces the highest susceptibility and affinity of the mats to 95%E and of the films to distilled water. Therefore, the here-developed mats and films appear to differ in affinity and stability in the media of different polarities, which might trigger the differences in phenolic compounds' migration.

Regarding RA, the highest migration occurred in 95%E from all formulations indicating that the chemical nature of the actives also influences migration behavior from the mats and films. Similarly, Talón et al. (2017) reported a higher RA migration from polysaccharides-based films to the food simulant with higher ethanol content due to decreased medium polarity and thus increased chemical affinity and solubility of RA in the medium. Of note, the higher RA migration in 10%E and 95%E occurred from the mats than the films. In the case of distilled water, the higher migration was from the films. This result confirms the above-mentioned different affinity and susceptibility of the mats and films to the media with different polarities, which results in a different rate of the matrices relaxation, media diffusion through the matrices, and the migration of the incorporated actives into the media.

According to the Regulation on plastic materials and articles intended to come into contact with food, phenolic compounds are not listed among substances with the provided specific migration limit nor other restrictions (European Commission, 2011). In that case, the generic specific migration limit of 60 mg/kg should apply. The amounts of migrated phenolic compounds from the developed ZG-based mats and films are below the provided generic specific migration limit and thus in line with the Regulation.

Altogether, the migration test revealed the ability of the ZG-based mats and films incorporating SE to deliver phenolics, recognized for active and bioactive properties, to foodstuff. This ability highlighted the potential of the developed mats and films for use as active food contact materials. Moreover, it showed that the phenolics' migration from the same formulation, in terms of the composition, could be tailored by the fabrication technique, depending on a specific application, i.e., the hydrophilic/lipophilic character of the food.

3.2.10. Antioxidant activity

After being incubated in DPPH• free radicals solution, the mats and films remained their integrity. All formulations exhibited an ability to scavenge DPPH• radicals when in direct contact (Table 3). The control mat and film showed the lowest DPPH• scavenging ability, which can originate from some protein fractions with antioxidant properties (amino acid residues, short peptides, and xanthophyll pigments of zein (Gagliardi et al., 2021), and peptide fractions of gelatin (Gómez-Estaca et al., 2009)). The mats' and films' ability to scavenge DPPH• radicals significantly increased ($p < 0.05$) with the SE incorporation and its increased content due to the SE intrinsic antioxidant activity. Positive effects of the SE incorporation on antioxidant properties of poly(ε-caprolactone)-based films (Salević et al., 2019), as well zein-based films and fibers (Salević et al., 2022), were also achieved. The sage antioxidative properties are primarily related to phenolic compounds, including phenolic acids. The chemical structure of phenolic acids is responsible for their free radicals scavenging ability. Namely, the hydroxyl groups have electron-donating properties, while conjugated unsaturation facilitates free radicals delocalization. Specifically, RA is an excellent DPPH• radical scavenger and one of the most potent antioxidant sage constituents (Farhat et al., 2013; Lamien-Meda et al., 2010; Lu & Foo, 2001). Accordingly, the obtained results suggest not only retained radicals scavenging ability of the SE during mats' and films' fabrication but also synergistic antioxidant activity of the protein matrix and incorporated extract.

Table 3
Biological activity of the ZG-based mats and films.

Sample	Antioxidant activity	Antibacterial activity			
	DPPH• inhibition (%)	*S. aureus* $\log_{10}$ (CFU/mL)	CFU reduction (R)	*E. coli* $\log_{10}$ (CFU/mL)	CFU reduction (R)
Bacterial suspension		8.39 ± 0.07^{a}	–	9.48 ± 0.00^{a}	–
ZGe	17.98 ± 0.90^{a}	6.03 ± 0.11^{b}	2.36 ± 0.12	9.00 ± 0.00^{a}	0.48 ± 0.00
ZG-5SEe	65.62 ± 2.83^{b}	5.48 ± 0.12	2.91 ± 0.12	7.79 ± 0.36^{b}	1.69 ± 0.36
ZG-10SEe	89.38 ± 2.24^{c}	5.39 ± 0.13^{ce}	3.00 ± 0.13	6.98 ± 0.02^{c}	2.49 ± 0.01
Bacterial suspension		8.39 ± 0.07^{a}	–	9.11 ± 0.00^{a}	–
ZGsc	10.46 ± 0.05^{d}	6.08 ± 0.50^{bd}	2.31 ± 0.50	6.63 ± 0.67^{c}	2.49 ± 0.68
ZG-5SEsc	43.83 ± 2.79^{e}	4.75 ± 0.38^{e}	3.64 ± 0.38	6.34 ± 0.34^{c}	2.77 ± 0.34
ZG-10SEsc	73.10 ± 1.87^{f}	3.88 ± 0.25	4.51 ± 0.25	5.19 ± 0.71^{d}	3.92 ± 0.71

Different letters within the same column indicate significant differences ($p < 0.05$).

The fabrication technique also influenced the radical scavenging ability of the samples, with the electrospun mats being more potent ($p < 0.05$) than the respective solvent-cast films, which underlines the dependence of the materials' properties on their structure, as already discussed. Thus, the high surface area of the fibrous mats may provide more contact within the reaction solution making active constituents more available to react and neutralize the radicals than the compact films.

Generally, the antioxidative performance of the developed mats and films incorporating SE highlights their potential for use as active, food contact materials with the functionality to prevent oxidative reactions and food deterioration or even impart health-beneficial effects.

3.2.11. Antibacterial activity

The antibacterial performance of the mats and films, i.e., the ability to reduce viable counts of foodborne pathogens when in direct contact, was tested against *S. aureus* and *E. coli*. All formulations exhibited antibacterial effects, regardless of the SE incorporation and fabrication technique (Table 3). It was interesting to observe the ability of the control mat and film to inhibit bacterial growth. These results initiated ion chromatography analysis of the suspensions after incubation with the samples to determine acetic-ion release from the mats and films and ex-

plain the antibacterial activity of the control samples. The IC showed the potential of the mats and films to bind acetic acid, used as a solvent for their synthesis, and release the acid into the suspensions during incubation. The concentrations of acetic-ion were 2.24, 1.78, and 2.02 mg/mL for the suspensions treated with ZGe, ZG-5SEe, and ZG-10SEe, respectively, and 1.94, 1.89, and 1.64 mg/mL for those treated with ZGsc, ZG-5SEsc, and ZG-10SEsc, respectively. Acetic acid is a weak digestible acid and an authorized food additive whose antibacterial activity is related to acidity and ability to diffuse through the membrane and cause cytoplasm acidification and changes to intracellular constituents (Contardi et al., 2017; European Parliament and the Council of the European Union, 2008). Similarly, Contardi et al. (2017) reported that acetic acid residues imparted activity against *E. coli* to polyvinylpyrrolidone-based mats and films. Apart from acetic acid residues, the swelling of zein-based mats and films may restrict available water and nutrients to bacteria and reduce their growth, which reflects in the antibacterial activity of the controls (Salević et al., 2022). The SE incorporation and increase in its content triggered more potent antibacterial efficiency of the mats and films. The antibacterial performance of the sage extract is highly related to phenolic compounds with multiple modes of action, via damage to the cell wall and membrane structures, changes in permeability, and leakage of intracellular components (Shan et al., 2007; Witkowska et al., 2013). Regarding PAs, their antibacterial action occurs via diffusion through the membrane, resulting in cytoplasm acidification and a decrease in cell viability (Sánchez-Maldonado et al., 2011). Accordingly, the antibacterial activity of the ZG-based mats and films incorporating SE could be ascribed to the synergistic effect of acetic acid residues and extract. SE incorporation also induced antibacterial activity of other materials, such as zein-based films and mats (Salević et al., 2022) and poly(ε-caprolactone) annealed films (Salević et al., 2019).

Generally, bacteria growth inhibition or CFU decrease by materials during 24 h incubation represents the bacteriostatic effect. CFU reduction of $\geq 3 \log_{10}$ defines as the bactericidal effect (Castro-Mayorga et al., 2017). Accordingly, the effect against *S. aureus* was bacteriostatic by ZGe, ZG-5SEe, and ZGsc and bactericidal by ZG-10SEe, ZG-5SEsc, and ZG-10SEsc formulations. Regarding *E. coli*, the effect was bacteriostatic, except for the ZG-10SEsc formulation, which generated a bactericidal effect. *S. aureus* was more susceptible than *E. coli*, regardless of the SE incorporation and fabrication technique, which is consistent with the antibacterial performance of the unloaded extract (Salević et al., 2019). It can be related to the more complex structure of Gram-negative bacteria than G-positive ones. Gram-negative bacteria have an outer membrane rich in lipopolysaccharides and periplasmic space with enzymes that may restrict the penetration of the outside molecules and inactivate the introduced molecules increasing bacterial resistance to actives (Shan et al., 2007).

The formulations with the same composition and different structures exhibited different bacterial growth inhibition, i.e., the solvent-cast films were more effective than the electrospun mats. A much higher density of solid films than fibrous mats caused by different morphologies (Tijing et al., 2013) could be responsible for the differences in the antibacterial activity of their surfaces. Accordingly, it seems that the surface density of actives is higher for the solvent-cast films, which may increase the actives' availability and antibacterial efficiency of the films' surfaces.

Altogether, the results highlighted the potential of the SE incorporation to impart antibacterial, apart from the antioxidant performance to the ZG-based mats and films, which could be of great interest regarding applications as active food contact materials aimed to preserve food quality and safety and decrease food waste generation.

3.2.12. Bio-disintegration in compost

The bio-disintegration of the mats and films during incubation in a compost model system was studied. The samples were periodically taken out from the compost and analyzed by comparing the visual appearance and measuring weight loss as a function of time (Fig. 4). All formulations showed rapid bio-disintegration, regardless of the fabrication technique and incorporation of the extract with antibacterial activity. There were fluctuations in weight loss during the time, as it could not be determined accurately due to compost particles adhering to the residual samples.

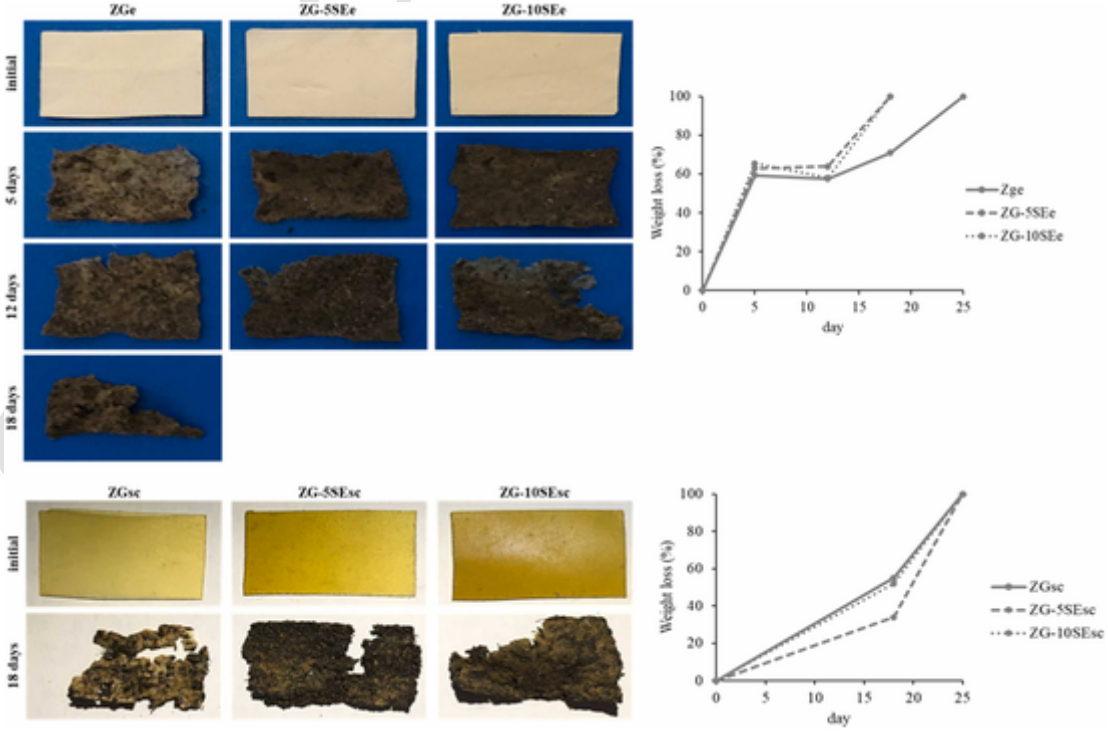

Fig. 4. Bio-disintegration images (left) and weight loss curves (right) of the electrospun mats and solvent-cast films during incubation in compost.

The electrospun mats showed evident changes, such as darkening, deformation, swelling, and fragmentation, indicating the beginning of the degradation after five days of incubation in compost. Further disintegration of the mats proceeded with incubation time, reaching the level without visible residues in the compost after 18–25 days. The SE incorporation had a positive effect and shortened the period needed for the complete disintegration of the resulting mats (18 days) compared to the control mat (25 days). Similarly, Medina Jaramillo et al. (2016) reported fostering biodegradability of starch films after being incorporated with yerba mate extract due to the fast degradation of low-molecular-weight compounds of the natural extract. Regarding the solvent-cast films, all formulations exhibited similar disintegration behavior, regardless of the SE incorporation. The changes in the films indicating the beginning of degradation, such as loss of transparency, darkening, deformation, and fragmentation, were observed later compared to the mats, i.e., after 18 days of incubation. This difference can be related to the structural differences between the mats and films. Thus, fibrous structures of the mats with a high surface-to-volume ratio may provide a higher specific surface area and accessibility to soil microorganisms than compact films' structures. However, complete films' disintegration occurred by the 25th day of incubation, the same as for the mats. Xiong et al. (2008) also reported that the initial biodegradation of structurally different materials occurs at different rates, reaching the same biodegradation rates at a later stage, i.e., with an increase in degradable time. Namely, dense, compact structures might reduce the microorganisms' infiltration velocity and slow initial degradation, while further incubation destroys the compactness and its influence on the degradation rate. It seems that the bio-disintegration of the mats and films occurs through an inhomogeneous mechanism. Nevertheless, the obtained results highlighted the efficiency of the compost microorganisms and their enzyme systems to erode the surfaces and spread into the bulk, entirely breaking the mats and films. Of importance, incorporation of the extract with antibacterial activity did not diminish the disintegration. Generally, if material degradation of at least 90% by biological action occurs in less than 180 days, it can be considered biodegradable material (Alves-Silva et al., 2022). Accordingly, the short time for the complete disintegration of the developed mats and films in the compost makes them very promising as eco-friendly materials. The elimination of waste materials can increase the degree of circularity compared to the usual linear process.

4. Conclusions

Electrospinning and solvent casting techniques enabled the development of ZG-based mats and films incorporating phenolics-rich SE. The performed characterization gave an insight into the influence of the applied fabrication techniques, SE incorporation, and its content (5, 10%) on the materials' properties. The electrospun mats were white-colored, opaque, and structurally composed of dense fibers, while the solvent-cast films were transparent, with continuous and compact structures. The SE incorporation increased fibers' diameter and mats' thickness and provided more homogenous film surfaces. The analysis implied good constituents' compatibility, homogenous dispersion, and efficient SE incorporation within the mats and films with low-intensity chemical interactions. The thermal denaturation was primarily influenced by the fabrication technique, less by the SE incorporation. The solid films were more stable, requiring higher denaturation temperatures than the fibrous mats. In addition to this, the films presented higher resistance to mechanical stress, elongation that can withstand before the break, and water vapor barrier performance. The SE-incorporating mats and films showed phenolics delivery ability to the food simulant media influenced by the SE content, materials' structure, and medium polarity. Further, the SE incorporation improved the mats' and films' ability to scavenge DPPH$^{\bullet}$ radicals and inhibit *S. aureus* and *E. coli* bacteria growth. The electrospun mats showed better antioxidative properties, and the solvent-cast films had higher antibacterial activity. These results are interesting for different applications, highlighting an ability to tailor the materials' properties by changing their morphology. Finally, the mats' and films' bio-disintegration in compost was rapid, regardless of the fabrication technique and SE incorporation. Altogether, the results highlighted the potential of the developed mats and films for use as active, eco-friendly, and sustainable food packaging materials, aiming to preserve food quality and safety and decrease food and packaging waste generation.

Funding

This work was supported by the Ministry of Education, Science, and Technological Development, Republic of Serbia (grant numbers 451–03–68/2022–14/200116, 451–03–68/2022–14/200135).

CRediT authorship contribution statement

Ana Salević-Jelić: Conceptualization, Formal analysis, Investigation, Methodology, Software, Visualization, Writing – original draft. **Steva Lević**: Conceptualization, Data curation, Formal analysis, Investigation, Methodology, Software, Supervision, Validation, Writing – review & editing. **Dušica Stojanović**: Conceptualization, Data curation, Formal analysis, Investigation, Methodology, Supervision, Validation, Writing – review & editing. **Sanja Jeremić**: Data curation, Formal analysis, Methodology, Validation, Writing – review & editing. **Dunja Miletić**: Data curation, Formal analysis, Methodology, Validation, Writing – review & editing. **Milena Pantić**: Data curation, Formal analysis, Methodology, Validation, Writing – review & editing. **Vladimir Pavlović**: Formal analysis, Methodology, Software, Validation, Writing – review & editing. **Ivana Sredović Ignjatović**: Data curation, Formal analysis, Methodology, Software, Validation, Writing – review & editing. **Petar Uskoković**: Conceptualization, Data curation, Funding acquisition, Project administration, Resources, Supervision, Validation, Writing – review & editing. **Viktor Nedović**: Conceptualization, Data curation, Funding acquisition, Project administration, Resources, Supervision, Validation, Writing – review & editing.

Declaration of Competing Interest

The authors have no competing interests to declare.

Data availability

Data will be made available on request.

Appendix A. Supporting information

Supplementary data associated with this article can be found in the online version at doi:10.1016/j.fpsl.2023.101027.

References

Algellai, A.A., Tomić, N., Vuksanović, M.M., Dojčinović, M., Volkov-Husović, T., Radojević, V., & Heinemann, R.J. (2018). *Adhesion testing of composites based on Bis-GMA/TEGDMA monomers reinforced with alumina based fillers on brass substrate. Composites Part B: Engineering, 140*(July 2017), 164–173. https://doi.org/10.1016/j.compositesb.2017.12.034.

Altan, A., Aytac, Z., & Uyar, T. (2018). *Carvacrol loaded electrospun fibrous films from zein and poly(lactic acid) for active food packaging. Food Hydrocolloids, 81*, 48–59. https://doi.org/10.1016/j.foodhyd.2018.02.028.

Alves-Silva, G.F., Romani, V.P., & Martins, V.G. (2022). *Jatobá (Hymenaea stigonocarpa) pulp films: Properties, antioxidant potential and biodegradability. Food Packaging and Shelf Life, 34*, 100923. https://doi.org/10.1016/j.fpsl.2022.100923.

Amin, U., Kashif, M., Khan, I., Aslam, A., Nazir, A., Riaz, S., … Lorenzo, M. (2022). *Biodegradable active, intelligent, and smart packaging materials for food applications. Food Packaging and Shelf Life, 33*, 100903. https://doi.org/10.1016/j.fpsl.2022.100903.

Andrade, J., González-Martínez, C., & Chiralt, A. (2022). *Physical and active properties of*

poly (vinyl alcohol) films with phenolic acids as affected by the processing method. Food Packaging and Shelf Life, 33, 100855. https://doi.org/10.1016/j.fpsl.2022.100855.
ASTM (1995). *Standard test methods for water vapour transmission of materials. Standard designations. ASTM Annual book of ASTM standards* (pp. E96–E95). American Society fot Testing and Materials.,.
Bertolo, M.R.V., Dias, L.D., Oliveira Filho, J.G., de, Alves, F., Marangon, C.A., Amaro Martins, V., … Bogusz, S. (2022). *Central composite design optimization of active and physical properties of food packaging films based on chitosan/gelatin/pomegranate peel extract. Food Packaging and Shelf Life, 34*, 100986. https://doi.org/10.1016/j.fpsl.2022.100986.
Cao, N., Fu, Y., & He, J. (2007). *Preparation and physical properties of soy protein isolate and gelatin composite films. Food Hydrocolloids, 21*(7), 1153–1162. https://doi.org/10.1016/j.foodhyd.2006.09.001.
Castro-Mayorga, J.L., Fabra, M.J., Pourrahimi, A.M., Olsson, R.T., & Lagaron, J.M. (2017). *The impact of zinc oxide particle morphology as an antimicrobial and when incorporated in poly(3-hydroxybutyrate-co-3-hydroxyvalerate) films for food packaging and food contact surfaces applications. Food and Bioproducts Processing, 101*, 32–44. https://doi.org/10.1016/j.fbp.2016.10.007.
Contardi, M., Heredia-Guerrero, J.A., Perotto, G., Valentini, P., Pompa, P.P., Spanò, R., … Bayer, I.S. (2017). *Transparent ciprofloxacin-povidone antibiotic films and nanofiber mats as potential skin and wound care dressings. European Journal of Pharmaceutical Sciences, 104*, 133–144. https://doi.org/10.1016/j.ejps.2017.03.044.
Deng, L., Kang, X., Liu, Y., Feng, F., & Zhang, H. (2018). *Characterization of gelatin/zein films fabricated by electrospinning vs solvent casting. Food Hydrocolloids, 74*, 324–332. https://doi.org/10.1016/j.foodhyd.2017.08.023.
Deng, L., Li, Y., Feng, F., Wu, D., & Zhang, H. (2019). *Encapsulation of allopurinol by glucose cross-linked gelatin/zein nanofibers: Characterization and release behavior. Food Hydrocolloids, 94*, 574–584. https://doi.org/10.1016/j.foodhyd.2019.04.004.
Deng, L., Zhang, X., Li, Y., Que, F., Kang, X., Liu, Y., … Zhang, H. (2018). *Characterization of gelatin/zein nanofibers by hybrid electrospinning. Food Hydrocolloids, 75*, 72–80. https://doi.org/10.1016/j.foodhyd.2017.09.011.
Echegoyen, Y., Fabra, M.J., Castro-Mayorga, J.L., Cherpinski, A., & Lagaron, J.M. (2017). *High throughput electro-hydrodynamic processing in food encapsulation and food packaging applications: Viewpoint. Trends in Food Science and Technology, 60*, 71–79. https://doi.org/10.1016/j.tifs.2016.10.019.
Etxabide, A., Garrido, T., Uranga, J., Guerrero, P., & de la Caba, K. (2018). *Extraction and incorporation of bioactives into protein formulations for food and biomedical applications. International Journal of Biological Macromolecules, 120*, 2094–2105. https://doi.org/10.1016/j.ijbiomac.2018.09.030.
European Commission, 2011, Regulation (EU) No 10/2011 on plastic materials and articles intended to come into contact with food. Official Journal of the European Union, 2011(L 12/1).
European Commission, 2017, Regulation (EU) 2017/752 amending and correcting Regulation (EU) No 10/2011 on plastic materials and articles intended to come into contact with food. Official Journal of the European Union, 2017(L 113/18).
European Parliament and the Council of the European Union, 2008, Regulation (EC) No 1333/2008 of the European Parliament ans of the Council of 16 December 2998 on food additives. Official Journal of the European Union, L 354, 16–33.
Farhat, M.Ben, Landoulsi, A., Chaouch-Hamada, R., Sotomayor, J.A., & Jordán, M.J. (2013). *Characterization and quantification of phenolic compounds and antioxidant properties of Salvia species growing in different habitats. Industrial Crops and Products, 49*, 904–914. https://doi.org/10.1016/j.indcrop.2013.06.047.
Gagliardi, A., Paolino, D., Costa, N., Fresta, M., & Cosco, D. (2021). *Zein- vs PLGA-based nanoparticles containing rutin: A comparative investigation. Materials Science and Engineering C, 118*, 111538. https://doi.org/10.1016/j.msec.2020.111538.
Gaona-Sánchez, V.A., Calderón-Domínguez, G., Morales-Sánchez, E., Chanona-Pérez, J.J., Velázquez-de la Cruz, G., Méndez-Méndez, J.V., … Farrera-Rebollo, R.R. (2015). *Preparation and characterisation of zein films obtained by electrospraying. Food Hydrocolloids, 49*, 1–10. https://doi.org/10.1016/j.foodhyd.2015.03.003.
Gómez-Estaca, J., Bravo, L., Gómez-Guillén, M.C., Alemán, A., & Montero, P. (2009). *Antioxidant properties of tuna-skin and bovine-hide gelatin films induced by the addition of oregano and rosemary extracts. Food Chemistry, 112*(1), 18–25. https://doi.org/10.1016/j.foodchem.2008.05.034.
Hernández-García, E., Vargas, M., & Chiralt, A. (2022). *Effect of active phenolic acids on properties of PLA-PHBV blend films. Food Packaging and Shelf Life, 33*, 100894. https://doi.org/10.1016/j.fpsl.2022.100894.
Jayakumar, A., Radoor, S., Kim, J.T., Rhim, J.W., Nandi, D., Parameswaranpillai, J., & Siengchin, S. (2022). *Recent innovations in bionanocomposites-based food packaging films – A comprehensive review. Food Packaging and Shelf Life, 33*, 100877. https://doi.org/10.1016/j.fpsl.2022.100877.
Kaewprachu, P., Osako, K., Benjakul, S., & Rawdkuen, S. (2015). *Quality attributes of minced pork wrapped with catechin-lysozyme incorporated gelatin film. Food Packaging and Shelf Life, 3*, 88–96. https://doi.org/10.1016/j.fpsl.2014.11.002.
Krstić, M., Radojević, M., Stojanović, D., Radojević, V., Uskoković, P., & Ibrić, S. (2017). *Formulation and characterization of nanofibers and films with carvedilol prepared by electrospinning and solution casting method. European Journal of Pharmaceutical Sciences, 101*, 160–166. https://doi.org/10.1016/j.ejps.2017.02.006.
Lamien-Meda, A., Nell, M., Lohwasser, U., Börner, A., Franz, C., & Novak, J. (2010). *Investigation of antioxidant and rosmarinic acid variation in the sage collection of the genebank in gatersleben. Journal of Agricultural and Food Chemistry, 58*(6), 3813–3819. https://doi.org/10.1021/jf903993f.
Li, L., Wang, H., Chen, M., Jiang, S., Cheng, J., Li, X., … Jiang, S. (2020). *Gelatin/zein fiber mats encapsulated with resveratrol: Kinetics, antibacterial activity and application for pork preservation. Food Hydrocolloids, 101*, 105577. https://doi.org/10.1016/j.foodhyd.2019.105577.
Liu, J., Yong, H., Liu, Y., Qin, Y., Kan, J., & Liu, J. (2019). *Preparation and characterization of active and intelligent films based on fish gelatin and haskap berries (Lonicera caerulea L.) extract. Food Packaging and Shelf Life, 22*(July), 100417. https://doi.org/10.1016/j.fpsl.2019.100417.
Liu, Y., Deng, L., Zhang, C., Chen, K., Feng, F., & Zhang, H. (2018). *Comparison of ethyl cellulose–gelatin composite films fabricated by electrospinning versus solvent casting. Journal of Applied Polymer Science, 135*(46), 1–10. https://doi.org/10.1002/app.46824.
Lu, Y., & Foo, L.Y. (2001). *Antioxidant activities of polyphenols from sage (Salvia officinalis). Food Chemistry, 75*, 197–202.
Malagurski, I., Levic, S., Nesic, A., Mitric, M., Pavlovic, V., & Dimitrijevic-Brankovic, S. (2017). *Mineralized agar-based nanocomposite films: Potential food packaging materials with antimicrobial properties. Carbohydrate Polymers, 175*, 55–62. https://doi.org/10.1016/j.carbpol.2017.07.064.
Martins, N., Barros, L., Santos-Buelga, C., Henriques, M., Silva, S., & Ferreira, I.C.F.R. (2014). *Evaluation of bioactive properties and phenolic compounds in different extracts prepared from Salvia officinalis L. Food Chemistry, 170*, 378–385. https://doi.org/10.1016/j.foodchem.2014.08.096.
Medina Jaramillo, C., Gutiérrez, T.J., Goyanes, S., Bernal, C., & Famá, L. (2016). *Biodegradability and plasticizing effect of yerba mate extract on cassava starch edible films. Carbohydrate Polymers, 151*, 150–159. https://doi.org/10.1016/j.carbpol.2016.05.025.
Melendez-Rodriguez, B., Figueroa-Lopez, K.J., Bernardos, A., Martínez-Máñez, R., Cabedo, L., Torres-Giner, S., & Lagaron, J.M. (2019). *Electrospun antimicrobial films of poly(3-hydroxybutyrate-co-3-hydroxyvalerate) containing eugenol essential oil encapsulated in mesoporous silica nanoparticles. Nanomaterials, 9*(2). https://doi.org/10.3390/nano9020227.
Mellinas, C., Valdés, A., Ramos, M., Burgos, N., Garrigos, M., & Jiménez, A. (2016). *Active edible films: Current state and future trends. Journal of Applied Polymer Science, 133*(2). https://doi.org/10.1002/app.42971.
Meng, Y., & Cloutier, S. (2014). *Gelatin and Other Proteins for Microencapsulation. Microencapsulation in the Food Industry*. Elsevier Inc,. https://doi.org/10.1016/b978-0-12-404568-2.00020-0.
Menges, F., 2018, Spectragryph - optical spectroscopy software (Version 1.2.8, 2018). http://www.effemm2.de/spectragryph/.
Neo, Y.P., Ray, S., Jin, J., Gizdavic-Nikolaidis, M., Nieuwoudt, M.K., Liu, D., & Quek, S.Y. (2013). *Encapsulation of food grade antioxidant in natural biopolymer by electrospinning technique: A physicochemical study based on zein-gallic acid system. Food Chemistry, 136*(2), 1013–1021. https://doi.org/10.1016/j.foodchem.2012.09.010.
Núñez-Flores, R., Giménez, B., Fernández-Martín, F., López-Caballero, M.E., Montero, M.P., & Gómez-Guillén, M.C. (2013). *Physical and functional characterization of active fish gelatin films incorporated with lignin. Food Hydrocolloids, 30*(1), 163–172. https://doi.org/10.1016/j.foodhyd.2012.05.017.
Ponjavic, M., Nikolic, M.S., Nikodinovic-Runic, J., Jeremic, S., Stevanovic, S., & Djonlagic, J. (2017). *Degradation behaviour of PCL/PEO/PCL and PCL/PEO block copolymers under controlled hydrolytic, enzymatic and composting conditions. Polymer Testing, 57*, 67–77. https://doi.org/10.1016/j.polymertesting.2016.11.018.
Rasid, N.A.M., Nazmi, N.N.M., Isa, M.I.N., & Sarbon, N.M. (2018). *Rheological, functional and antioxidant properties of films forming solution and active gelatin films incorporated with Centella asiatica (L.) urban extract. Food Packaging and Shelf Life, 18*(November 2017), 115–124. https://doi.org/10.1016/j.fpsl.2018.10.002.
Salević, A., Prieto, C., Cabedo, L., Nedović, V., & Lagaron, J.M. (2019). *Physicochemical, antioxidant and antimicrobial properties of electrospun poly(ε-caprolactone) films containing a solid dispersion of sage (Salvia officinalis L.) extract. Nanomaterials, 9*(2), 270. https://doi.org/10.3390/nano9020270.
Salević, A., Stojanović, D., Lević, S., Pantić, M., Đorđević, V., Pešić, R., … Nedović, V. (2022). *The Structuring of Sage (Salvia officinalis L.) Extract-Incorporating Edible Zein-Based Materials with Antioxidant and Antibacterial Functionality by Solvent Casting versus Electrospinning. Foods, 11*(3), 390. https://doi.org/10.3390/foods11030390.
Sánchez-Maldonado, A.F., Schieber, A., & Gänzle, M.G. (2011). *Structure-function relationships of the antibacterial activity of phenolic acids and their metabolism by lactic acid bacteria. Journal of Applied Microbiology, 111*(5), 1176–1184. https://doi.org/10.1111/j.1365-2672.2011.05141.x.
Shan, B., Cai, Y.Z., Brooks, J.D., & Corke, H. (2007). *The in vitro antibacterial activity of dietary spice and medicinal herb extracts. International Journal of Food Microbiology, 117*(1), 112–119. https://doi.org/10.1016/j.ijfoodmicro.2007.03.003.
Shan, B., Cai, Y.Z., Sun, M., & Corke, H. (2005). *Antioxidant capacity of 26 spice extracts and characterization of their phenolic constituents. Journal of Agricultural and Food Chemistry, 53*(20), 7749–7759. https://doi.org/10.1021/jf051513y.
Singleton Vernon, L., O. R., & Lamuela-Raventos, R.M. (1999). *Analysis of total phenols and other oxidation substrates and antioxidants by means of Folin-Ciocalteu reagent. Methods in Enzymology*: *Vol. 299* (pp. 152–178). Massachusetts, United States: Academic Press,. https://doi.org/10.1016/S0076-6879(99)99017-1.
Tagrida, M., Nilsuwan, K., Gulzar, S., Prodpran, T., & Benjakul, S. (2023). *Fish gelatin/chitosan blend films incorporated with betel (Piper betle L.) leaf ethanolic extracts: Characteristics, antioxidant and antimicrobial properties. Food Hydrocolloids, 137* (October 2022), 108316. https://doi.org/10.1016/j.foodhyd.2022.108316.
Talón, E., Trifkovic, K.T., Vargas, M., Chiralt, A., & González-Martínez, C. (2017). *Release of polyphenols from starch-chitosan based films containing thyme extract. Carbohydrate Polymers, 175*, 122–130. https://doi.org/10.1016/j.carbpol.2017.07.067.
Tijing, L.D., Park, C.H., Choi, W.L., Ruelo, M.T.G., Amarjargal, A., Pant, H.R., … Kim, C.S. (2013). *Characterization and mechanical performance comparison of multiwalled carbon nanotube/polyurethane composites fabricated by electrospinning and solution casting. Composites Part B: Engineering, 44*(1), 613–619. https://doi.org/10.1016/j.compositesb.2012.02.015.
Trifković, K., Milašinović, N., Djordjević, V., Zdunić, G., Kalagasidis Krušić, M.,

Knežević-Jugović, Z., … Bugarski, B. (2015). *Chitosan crosslinked microparticles with encapsulated polyphenols: Water sorption and release properties*. *Journal of Biomaterials Applications*, *30*(5), 618–631. https://doi.org/10.1177/0885328215598940.

Wang, D., Sun, J., Li, J., Sun, Z., Liu, F., Du, L., & Wang, D. (2022). *Preparation and characterization of gelatin/zein nanofiber films loaded with perillaldehyde, thymol, or ε-polylysine and evaluation of their effects on the preservation of chilled chicken breast*. *Food Chemistry*, *373*, 131439. https://doi.org/10.1016/j.foodchem.2021.131439.

Witkowska, A.M., Hickey, D.K., Alonso-Gomez, M., & Wilkinson, M. (2013). *Evaluation of antimicrobial activities of commercial herb and spice extracts against selected food-borne bacteria*. *Journal of Food Research*, *2*(4), 37. https://doi.org/10.5539/jfr.v2n4p37.

Wu, J., Chen, S., Ge, S., Miao, J., Li, J., & Zhang, Q. (2013). *Preparation, properties and antioxidant activity of an active film from silver carp (Hypophthalmichthys molitrix) skin gelatin incorporated with green tea extract*. *Food Hydrocolloids*, *32*(1), 42–51. https://doi.org/10.1016/j.foodhyd.2012.11.029.

Xiong, H.G., Tang, S.W., Tang, H.L., & Zou, P. (2008). *The structure and properties of a starch-based biodegradable film*. *Carbohydrate Polymers*, *71*(2), 263–268. https://doi.org/10.1016/j.carbpol.2007.05.035.

Yemenicioğlu, A. (2016). *Zein and its composites and blends with natural active compounds: development of antimicrobial films for food packaging*. *Antimicrobial Food Packaging*, 503–513. https://doi.org/10.1016/B978-0-12-800723-5.00041-3.

Zhang, X., Ma, L., Yu, Y., Zhou, H., Guo, T., Dai, H., & Zhang, Y. (2019). *Physico-mechanical and antioxidant properties of gelatin film from rabbit skin incorporated with rosemary acid*. *Food Packaging and Shelf Life*, *19*(2), 121–130. https://doi.org/10.1016/j.fpsl.2018.12.006.